Bifurcation Properties of a Stratospheric Vacillation Model

SHIGEO YODEN*,†

Department of Atmospheric Sciences, University of Washington, Seattle, WA 98195

(Manuscript received 20 August 1986, in final form 29 December 1986)

ABSTRACT

Nonlinear properties of a stratospheric vacillation model are investigated numerically in the light of bifurcation theory. The model is exactly the same as that used by Holton and Mass, which describes the wave–zonal flow interaction in a β-channel under a nonconservative constraint with zonal-flow forcing and wave dissipation. A set of 81 nonlinear ordinary differential equations with variables depending on time is obtained by a severe truncation and vertical differencing. All of the external parameters are fixed in time. The amplitude of the wave forcing or the intensity of zonal wind forcing at the bottom boundary is changed as a bifurcation parameter.

Three branches of the steady solutions are obtained by use of Powell's hybrid method and the pseudo-arclength continuation method. Linear stability of these solution branches is investigated by solving an eigenvalue problem in the linearized system. In some range of the bifurcation parameter, there exists a multiplicity of stable steady solutions with different vertical structures.

Periodic solutions, a series of stratospheric vacillations originally found by Holton and Mass, are obtained by time-integrations. It is found that the periodic solutions branch off from a steady solution by a Hopf bifurcation. For a finite increment of the parameter from the bifurcation point, the time average of the periodic solution is significantly different from the unstable steady solution. The nonlinear transience causes the difference.

The multiplicity of stable solutions (steady and periodic) is a possible explanation for the interannual variability of the stratospheric circulation in the middle and high latitudes during winter.

1. Introduction

Holton and Mass (1976) and Holton and Dunkerton (1978) (hereafter referred to as HM and HD, respectively) brought a new paradigm into the theory on time-variations of the planetary flow in the stratosphere (i.e., sudden stratospheric warmings and vacillations). By using a simplified quasi-geostrophic β-channel model, they concluded that "oscillations in stratospheric long waves do not necessarily reflect oscillating tropospheric forcing but may occur even in the presence of steady forcing." Another important result (HD) is the sensitivity of the onset of vacillation to the external parameters such as the amplitude of wave forcing and the mean-flow profile in the radiative equilibrium of the Newtonian heating.

Recently, Chao (1985) investigated the HM model by time integrations in which he gradually increased or decreased the amplitude of wave forcing. He obtained a hysteretic property which supported the sensitivity of the onset of vacillation. He conjectured that the hysteresis could be understood as a catastrophe and that the sudden warmings could be explained by the catastrophe theory.

Chao's numerical experiments were motivated by the pioneering work by Charney and DeVore (1979) on the multiple stable states in quasi-geostrophic barotropic flow over bottom topography, which was aimed at an explanation of the blocking mechanism. Charney and DeVore (1979) emancipated nonlinear dynamic meteorology from fetters of initial value problems. Many people followed them by using less severely truncated models, weakly nonlinear theories and baroclinic two-layer models. At present it is not difficult to apply a similar numerical procedure to nonlinear systems with an order of 10^2 degrees of freedom (Yoden, 1985).

In this paper we will apply the numerical analysis procedure pioneered by Charney and DeVore (1979) to the stratospheric vacillation model introduced by HM and HD. The HM model is reviewed in section 2. Numerical procedures are described in section 3 and results shown in section 4. Relation to some model studies of stratospheric dynamics and application of the results to the real stratosphere are discussed in section 5. Section 6 gives the conclusion.

2. Model description

The model is exactly the same as that used by HD, which has a different top boundary condition from the original HM model. In these studies the geostrophic

* Japan Society for the Promotion of Science Fellow for Research Abroad.

† Permanent affiliation: Geophysical Institute, Kyoto University, Kyoto, 606 Japan.

streamfunction for a wave ψ' and the mean zonal wind $\bar{u}$ are assumed as follows:

$$\psi'(x,y,z,t) = \mathrm{Re}[\Psi(z,t)e^{ikx}]e^{z/2H}\sin ly, \quad (2.1)$$

$$\bar{u}(y,z,t) = U(z,t)\sin ly. \quad (2.2)$$

In this paper we fundamentally use the same notations as those in HM and HD. The equation for the conservation of quasi-geostrophic potential vorticity and the mean-flow equation become, respectively,

$$\left(\frac{\partial}{\partial t}+ik\epsilon U\right)\left[-(k^2+l^2)+\frac{f_0^2}{N^2}\left(\frac{\partial^2}{\partial z^2}-\frac{1}{4H^2}\right)\right]\Psi + \beta'_e ik\Psi + \frac{f_0^2}{N^2}\left(\frac{\partial}{\partial z}-\frac{1}{2H}\right)\left[\alpha\left(\frac{\partial}{\partial z}+\frac{1}{2H}\right)\Psi\right]=0, \quad (2.3)$$

$$\frac{1}{\epsilon}\frac{\partial \beta'_e}{\partial t} = \frac{f_0^2}{N^2}\left(\frac{\partial}{\partial z}-\frac{1}{H}\right)\left[\alpha\left(\frac{\partial U}{\partial z}-\frac{dU_R}{dz}\right)\right] + \frac{1}{2}kl^2\epsilon\frac{f_0^2}{N^2}e^{z/H}\,\mathrm{Im}\left[\Psi^*\frac{\partial^2\Psi}{\partial z^2}\right], \quad (2.4)$$

where

$$\beta'_e = \beta + l^2\epsilon U - \epsilon\frac{f_0^2}{N^2}\left(\frac{\partial^2 U}{\partial z^2}-\frac{1}{H}\frac{\partial U}{\partial z}\right). \quad (2.5)$$

The flow is assumed to be confined to a β-channel centered at 60°N with a meridional extent of 60° latitude (i.e., $f_0 = 1.26\times10^{-4}$ s^{-1}, $\beta = 1.14\times10^{-11}$ m^{-1} s^{-1}, $l = 3/a = 4.71\times10^{-7}$ m^{-1}, and a is radius of the earth). Wave forcing is given by a zonal planetary wavenumber 2($k = 2/(a\cos60°) = 6.28\times10^{-7}$ m^{-1}). A constant ϵ comes from the truncation of nonlinear terms [$\epsilon = 8/(3\pi)$].

We set the static stability N^2 and the scale height H constant: $N^2 = 4\times10^{-4}$ s^{-2}, $H = 7\times10^3$ m. A Newtonian heating/cooling scheme is incorporated to generate the mean zonal wind and to dissipate the wave. The Newtonian heating/cooling coefficient α is given by

$$\alpha(z) = \{1.5+\tanh[(z-25)/7]\}\times10^{-6}\,\mathrm{s}^{-1}, \quad (2.6)$$

where z is given in kilometers. A simple radiative equilibrium state U_R is assumed for the mean zonal wind:

$$U_R(z) = U_{RB} + \Lambda z. \quad (2.7)$$

The top and bottom boundary conditions are given by

$$\Psi(z_T,t) = 0, \quad (2.8a)$$

$$\left.\frac{\partial U}{\partial z}\right|_{z=z_T} = \left.\frac{dU_R}{dz}\right|_{z=z_T}, \quad (2.8b)$$

and

$$\Psi(0,t) = gh_B/f_0, \quad (2.9a)$$

$$U(0,t) = U_R(0). \quad (2.9b)$$

It is assumed that the Newtonian heating equals zero at the top boundary (2.8b). Throughout this study the amplitude of the wave forcing at the bottom is held constant in time (2.9a) except in a discussion of Fig. 8, because we are not interested in a transient response to amplifying or decaying wave forcings but in the simplest case of steady forcing.

For computational convenience we put

$$\Psi(z,t) = A(z,t) + iB(z,t), \quad A \text{ and } B \text{ real}, \quad (2.10)$$

and decompose the equation (2.3) into two real differential equations for $A(z,t)$ and $B(z,t)$.

We set up the finite differencing by letting $z = j\Delta z$, where $j = 0, 1, \cdots, J$; J corresponds to the top boundary, $z_T = J\Delta z$. First and second differentials with respect to z are replaced with centered differences:

$$\left.\frac{\partial X}{\partial z}\right|_{z=j\Delta z} = \frac{X_{j+1}-X_{j-1}}{2\Delta z}, \quad (2.11a)$$

$$\left.\frac{\partial^2 X}{\partial z^2}\right|_{z=j\Delta z} = \frac{X_{j+1}-2X_j+X_{j-1}}{\Delta z^2}, \quad (2.11b)$$

where $X_l(t) = X(l\Delta z, t)$ and X is A, B or U.

By the finite vertical differencing, we finally obtain a set of nonlinear ordinary differential equations for $3(J-1) = N$ variables. If we define Φ as

$$\Phi(t) = (\phi_n(t))^{\mathrm{T}} = (A_1, A_2, \cdots, A_{J-1}, B_1, \cdots, B_{J-1}, U_1, \cdots, U_{J-1})^{\mathrm{T}}, \quad (2.12)$$

the set of equations can be written in tensor form:

$$\mathbf{M}\frac{d\Phi}{dt} = \Phi^{\mathrm{T}}\mathbf{N}\Phi + \mathbf{L}\Phi + C. \quad (2.13)$$

The righthand side of (2.13) comes from the local time change in (2.3) and (2.4). The nonlinear term $\Phi^{\mathrm{T}}\mathbf{N}\Phi$ is a potential vorticity advection by the mean zonal flow in (2.3) and the wave effect (horizontal heat flux convergence) on the mean zonal flow in (2.4). The β-term and the Newtonian dampings constitute the linear term $\mathbf{L}\Phi$. The constant C comes from the Newtonian heating term. The system described by (2.13) is a forced-dissipative system, because the mean zonal wind is forced by the Newtonian heating and the wave is dissipated by the thermal damping.

3. Method of numerical analysis

a. Bifurcation parameters and critical points

Fundamentally critical points (e.g., bifurcation point, limit point, transcritical point, . . .) in the Navier–Stokes equations are classified by considering the symmetry breaking in the velocity field (Matsuda, 1983). Some of the critical points are shown in Fig. 1. If we take note of the spatial symmetry in the HM model, we can expect the critical points which may exist in the model. An external forcing, in this case the wave forcing, has the lowest spatial symmetry. Hence, there

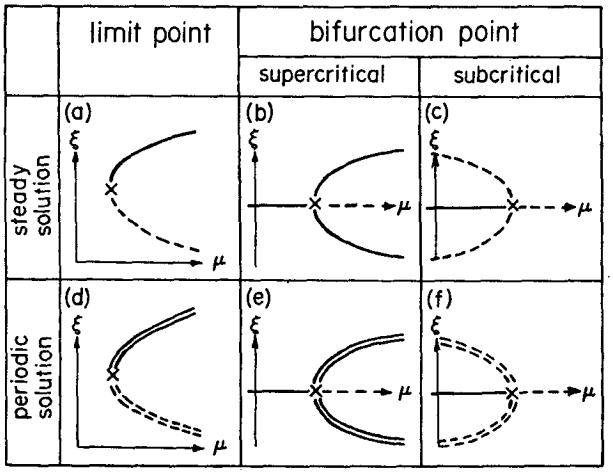

FIG. 1. Schematic diagram of some critical points. Two axes μ and ξ are the bifurcation parameter and a dependent variable in the system, respectively. Solid line is a stable steady solution branch and broken line an unstable one. Double solid line and double broken line are stable and unstable periodic solution branch, respectively. Critical point is indicated by ×. Bifurcation of periodic solutions from a steady solution is called Hopf bifurcation [(e) and (f)].

is no subsystem in Eq. (2.13). As a result, bifurcation points of the steady solution (Fig. 1b, c) may not exist. Other critical points may exist.

As a bifurcation parameter (μ in Fig. 1), we take the amplitude of wave forcing h_B at the bottom boundary; the dependence of steady solutions and time-dependent solutions on the parameter is investigated. The intensity of zonal wind forcing at the bottom boundary will be adopted as another bifurcation parameter in section 5 in order to obtain some relation to resonance theory.

Time-integration with constant and slow increase of the parameter h_B (Chao, 1985) is a reasonable way to obtain a rough estimate of the critical points. Table 1 shows the critical amplitude of h_B for transition to vacillations when the parameter is increased linearly with 0.5 m day^{-1}. The critical value becomes large when Λ and U_{RB} increase (although there are some exceptions). In section 4, Λ and U_{RB} are fixed at 2 m s^{-1}/km and 10 m s^{-1}.

b. *Steady solutions*

A steady solution $\bar{\Phi}$ satisfies the simultaneous nonlinear algebraic equation: [rhs of (2.13)] = 0. Powell's hybrid method in the IMSL package was used to obtain $\bar{\Phi}$ with many different initial guesses to the roots.

In order to obtain steady solution branches in a parameter space, we adopted two continuation methods: 1) a trivial method with parallel projection and 2) the pseudo-arclength method used by Legras and Ghil (1985). The latter is efficacious around a limit point although it is much more CPU time-consuming than the former.

c. *Linear stability of steady solutions*

If we assume a small perturbation Φ' from the steady solution $\bar{\Phi}$, the equation (2.13) can be linearized for Φ':

$$\mathbf{M}\frac{d\Phi'}{dt} = \mathbf{K}\Phi', \tag{3.1}$$

where the rhs is a linear function of Φ',

$$\mathbf{K}\Phi' = \bar{\Phi}^{\mathrm{T}}\mathbf{N}\Phi' + \Phi'^{\mathrm{T}}\mathbf{N}\bar{\Phi} + \mathbf{L}\Phi'. \tag{3.2}$$

If the perturbation is a form of $\Psi e^{\sigma t}$, (3.1) gives an eigenvalue problem:

$$[\mathbf{M}^{-1}\mathbf{K} - \sigma]\Psi = 0. \tag{3.3}$$

Linear stability of the steady solution is investigated by obtaining eigenvalues and eigenvectors of the matrix $\mathbf{M}^{-1}\mathbf{K}$ with an IMSL routine.

d. *Time-dependent solutions*

We adopt a time-integration scheme described in HM to obtain periodic and nonperiodic solutions. Initial conditions are steady solutions with small perturbations. Integrations are continued long enough for the initial transience to dissipate out.

In this study we define a time average for one cycle of the periodic solutions. If we express the time average as $[\Phi]$ and the deviation from it as Φ^*, the time average of (2.13) becomes

$$0 = [\Phi]^{\mathrm{T}}\mathbf{N}[\Phi] + \mathbf{L}[\Phi] + C + [\Phi^{*\mathrm{T}}\mathbf{N}\Phi^*]. \tag{3.4}$$

4. Results

a. *Steady solutions and their stability*

First of all, steady solutions were searched for a given parameter h_B = 55 m with twenty different initial guesses. The solution converged into one of three steady solutions. Note that in general these three solutions are not all the steady solutions for the parameter but only some of them, because no method provides automatically the entire picture of all possible steady solutions (Legras and Ghil, 1985).

Figure 2 shows the vertical profile of each solution (A–C). The solution A is close to the radiative equilib-

TABLE 1. Critical amplitude of wave forcing (units = m) for various values of U_{RB} and Λ. It is defined as a value of h_B for which the mean zonal wind has a negative value at least one level when h_B is increased linearly for 0.5 m day^{-1}.

Λ (m s^{-1}/km)	U_{RB} (m s^{-1})			
	0	5	10	15
1	45	65	45	170
2	130	45	175	425
3	185	120	340	690

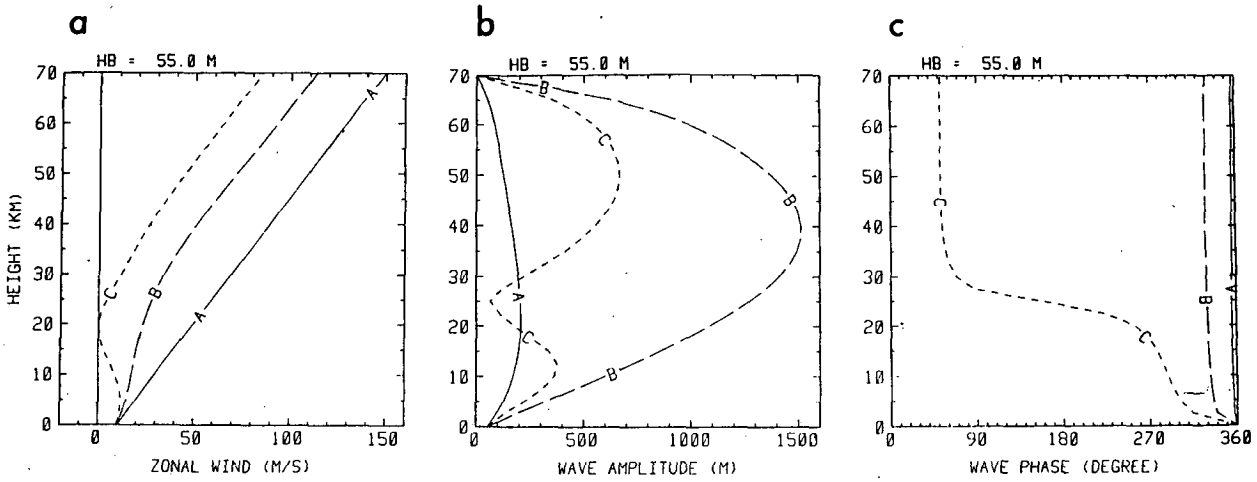

FIG. 2. Vertical profile of three steady solutions (A–C) for h_B = 55 m. Mean zonal wind (a), wave amplitude (b) and wave phase (c).

rium; the mean zonal wind is close to U_R, the wave amplitude is small and the westward tilt of the wave phase is also small. The solution B has weaker zonal winds and larger wave amplitudes than A. Mean zonal winds of the solution C have critical levels and just above these levels the wave has a nodal structure.

The steady solution branches in the parameter space were explored by two kinds of continuation methods from the foregoing steady solutions. The bifurcation diagram is shown in Fig. 3. Only the solution A is obtained for a small wave forcing h_B. As h_B increases, the wave amplitude increases while the mean zonal wind decreases. The branches A and B merge at the limit point L (h_B = 157 m). For a larger h_B, only the steady solution C is obtained, which has weak zonal winds and wave with a node.

The linear stability analysis of the steady solutions reveals that all of the steady solutions A are stable and all of B unstable. Because the solutions C are stable for 31.6 m < h_B < 32.6 m and 33.7 m < h_B < 59.4 m, there exists a multiplicity of stable steady solutions within these ranges.

b. *Time-dependent solutions*

At h_B = 59.4 m (H in Fig. 3) the solution C becomes unstable with complex conjugate eigenvalues. That is, a Hopf bifurcation takes place, which is a bifurcation of periodic solutions from the steady solution (Fig. 1e, f).

Some time integrations were performed to investigate the Hopf bifurcation. Figure 4 shows a trajectory of time-dependent solutions projected onto (A_{10}, $-B_{10}$) plane, which is a harmonic dial of the wave at the 25 km level. Below the critical value (h_B = 59.3 m), the trajectory shows attractions into the stable steady solution C (Fig. 4a), while just above the critical value (h_B = 59.5 m) there exists a periodic solution close to the unstable steady solution (Fig. 4b). The period is 103.9 days and equal to $2\pi/\mathrm{Im}[\sigma]$ (Fig. 5). This correspondence is a fundamental character of the Hopf bifurcation.

Note that we do not need to increase the wave forcing at the initial stage like HM. The initial conditions for the solutions shown in Fig. 4b–i are the unstable steady solution C with small perturbations and the wave forcing is fixed at a constant value from the initial state. The perturbations grow up owing to the instability and the time-dependent solutions are finally attracted into the periodic solutions.

As the wave forcing h_B increases, the periodic solution acquires large amplitude and changes its trajectory; the wave does not make a simple progression but a complex behavior with amplitude variations (Fig. 4c, d, . . .). The period becomes short as the parameter increases except for h_B < 61 m (Fig. 5). All of these solutions are purely periodic; chaotic solutions were not obtained in this study. These periodic solutions were named stratospheric vacillations in HM. Because these periodic solutions are stable (i.e., these are attractors), there exists a multiplicity of stable solutions (the steady solution A and the periodic solution) for 59.4 m < h_B < 157 m.

The time average and the range of the vacillations are shown in Fig. 3 by a diamond and a vertical bar, respectively. The time-averaged wave is also shown in Fig. 4 by a symbol Y. From these figures it is concluded that this is a case of the supercritical Hopf bifurcation (Fig. 1e).

It is also clear that the time average is significantly different from the unstable solution C when the parameter h_B exceeds the critical point finitely. Figure 6 shows the difference of the steady solution and the time-averaged state for h_B = 100 m. The difference of the wave structure is striking; the time-averaged wave, which is usually called a stationary component, has no node around the 20 km level. The amplitude in the

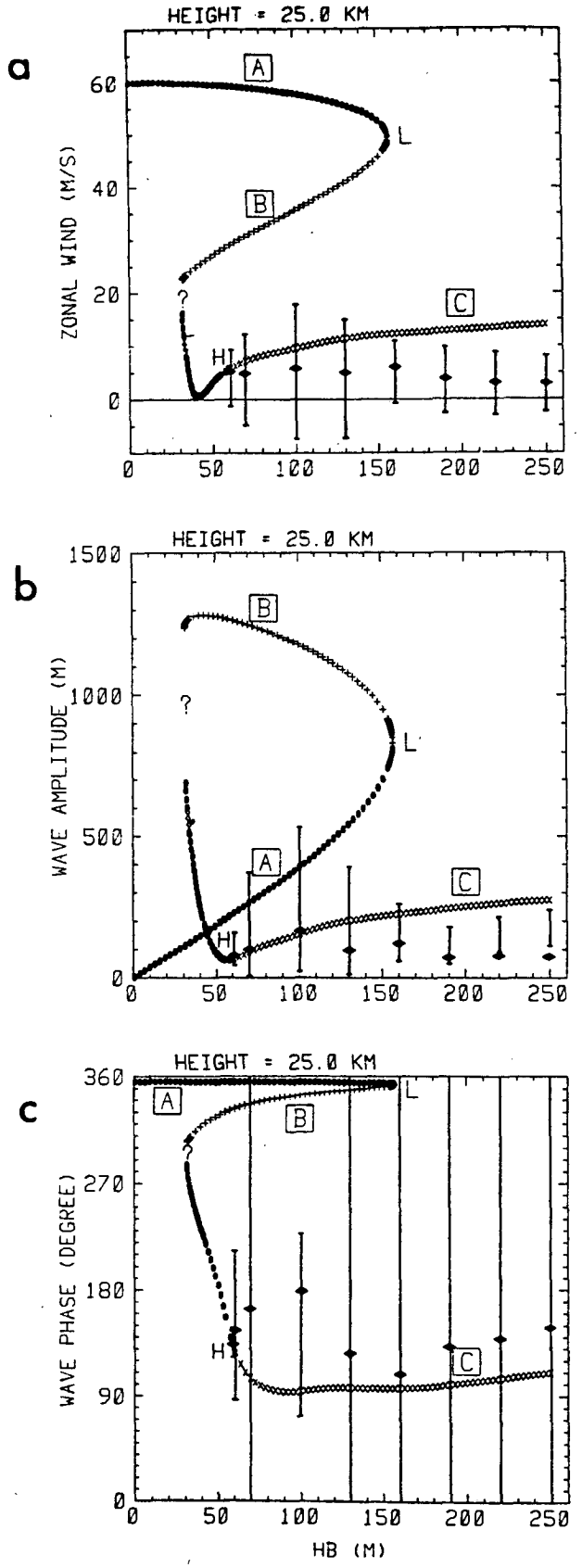

upper layers is smaller than the steady solution while the westward tilt of wave phase is larger.

The difference comes from the nonlinear transience term, i.e., $[\Phi^{*T}\mathbf{N}\Phi^{*}]$ in Eq. (3.4). Near the Hopf bifurcation point, this term is small and $\bar{\Phi} \approx [\Phi]$. However, it cannot be neglected for the parameter h_B far from the Hopf bifurcation point.

Physical aspects of the steady solutions and the periodic solutions will be investigated in a separate paper. Here we present only one figure to show the general features of the vacillations. Figure 7 gives time–height sections of the mean zonal wind U. Some of them remind us of "major warmings" [(c), (d) and (e)] and some others "minor warmings" [(b) and (f)]. Gradual buildup and rapid deceleration of the westerly winds are impressive in the cases of "major warmings."

5. Discussion

Multiplicity of stable solutions is possible in the HM model under appropriate external parameters (Fig. 3); one of them is close to the radiative equilibrium state; the other has weak zonal winds and large wave amplitudes in the lower layers. (The latter is either a steady solution or a vacillation.) It is interesting to refer to a recent GCM experiment and observational studies in relation to multiple stable states.

Boville (1986) performed a GCM experiment by using a model that extends to the lower mesosphere. Under perpetual January conditions (i.e., all of the external forcings are fixed in time), he obtained two qualitatively different planetary flow regimes. If we follow the terminology introduced by Labitzke (1977, 1982), the two regimes are "relatively undisturbed," cold winter and "disturbed", warm winter. In the undisturbed cold regime the polar night jet is strong, the polar region is cold and the wave activity small. On the other hand, the disturbed warm regime is opposite to the undisturbed cold regime.

It is difficult to relate our result in the simplest stratospheric model *directly* with that in a sophisticated GCM. However, it is interesting to mention a "coincidence" between them. The stable steady solution A in Figs. 2 and 3 has the characteristics of an undisturbed cold regime, while the steady solution C and the vacillation belong to the disturbed warm regime.

FIG. 3. Bifurcation diagram for the external paramater h_B (wave forcing at the bottom boundary). Mean zonal wind (a), wave amplitude (b), and wave phase (c) at the 25 km level. The stable steady solution is denoted by solid circles; unstable one by + or ×. The solution denoted by + has a pure real positive eigenvalue while that by × has a couple of complex conjugate eigenvalues with positive real part. Time average and range of periodic solutions are shown by a diamond and a vertical bar, respectively. The limit point is indicated by L and the Hopf bifurcation point by H. Exploration of the branches B and C were stopped at h_B = 31.6 m for an economical reason (indicated by ?).

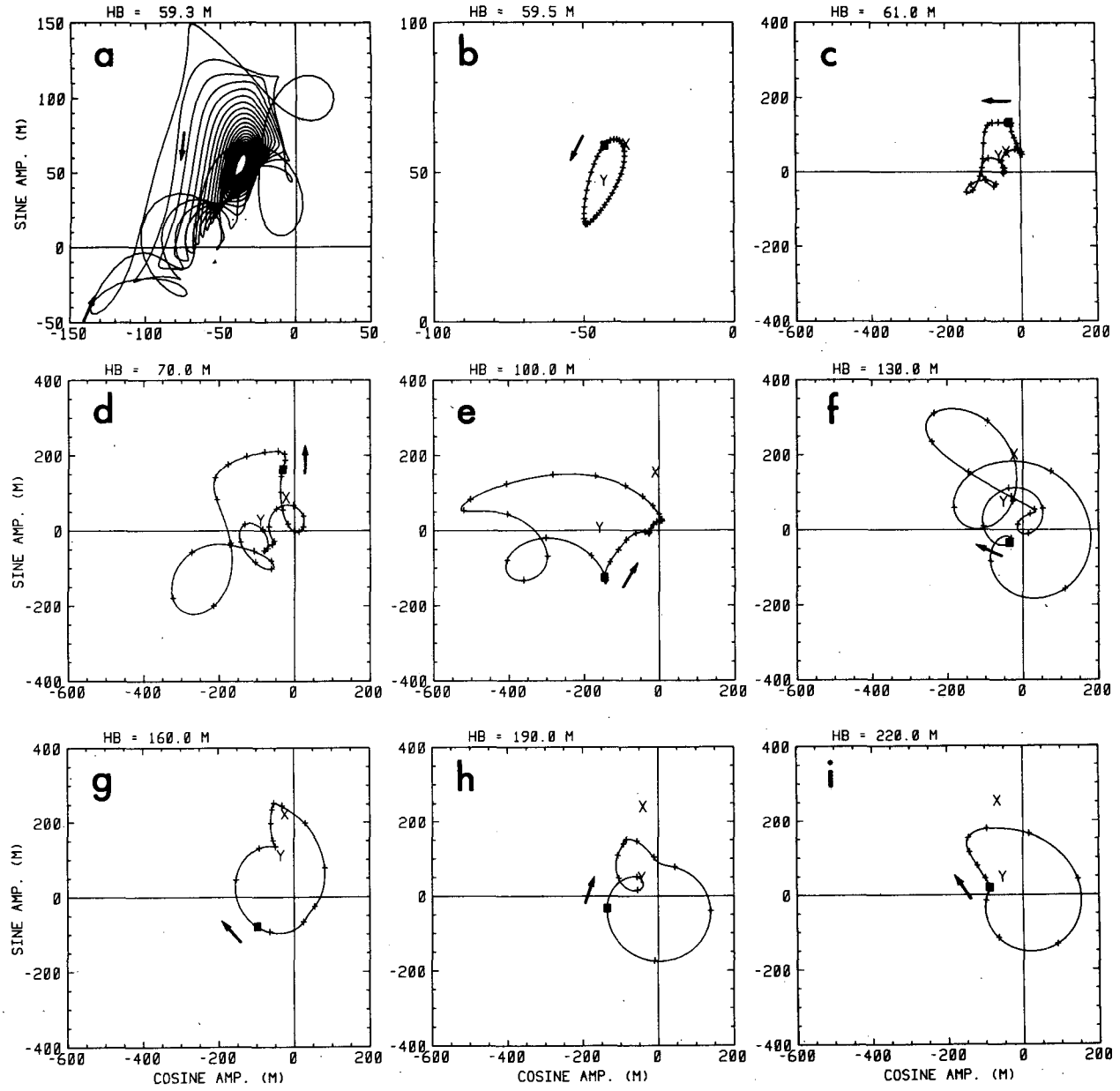

FIG. 4. Trajectory of time-dependent solutions projected onto (A_{10}, $-B_{10}$) plane. This is a harmonic dial of the wave at the 25 km level. Initial condition is the unstable steady solution B for the case *a* and C for *b–i* with small perturbations. In *b–i* the unstable steady solution C (and the initial state) is denoted by X and the time-averaged wave over one period by Y. The solid square on each trajectory corresponds to the time on the left edge in Fig. 7. Plus signs mark every third day after the square.

In the GCM experiment a transition from the undisturbed cold regime to the other was triggered by a sudden warming. This is an example of the almost-intransitive system defined by Lorenz (1968). On the other hand, in the present model it is impossible to transit from one stable solution to the other without changing the external parameters (i.e., the model is an intransitive system). Following Charney and DeVore (1979), however, we can hypothesize that in reality the states are metastable—unstable to smaller-scale perturbations— and that the instabilities act to produce an additional forcing which ultimately drives the flow system from the vicinity of one metastable state into that of another. Hence, the present model may be a conceptual model of the multiple planetary flow regimes in Boville's GCM.

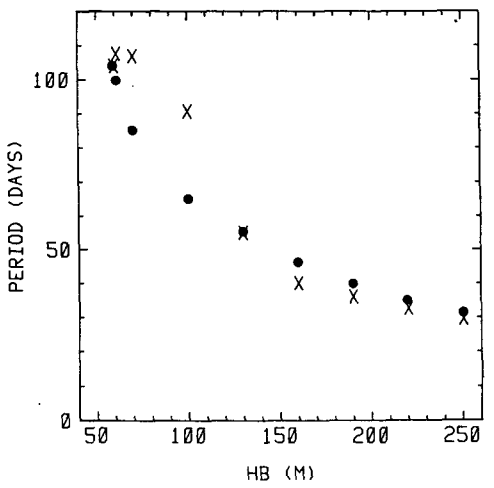

FIG. 5. Period of vacillations (×) and $2\pi/\mathrm{Im}[\sigma]$ (solid circle), where σ is a complex conjugate eigenvalue with positive real part for the unstable steady solution C.

In the real stratosphere, interannual variability during the northern winters may be related to multiple planetary flow regimes. Labitzke (1977, 1982) showed that one can distinguish between undisturbed cold winter months and disturbed warm ones. Holton and Tan (1980, 1982) and Labitzke (1982) pointed out their relation to the equatorial quasi-biennial oscillation (QBO). Shifts in the latitude of the critical line associated with the QBO was hypothesized to be responsible for the variability in high latitudes (Holton and Tan, 1980).

The shifts of the critical latitude might be roughly incorporated into the present model with a change of channel width. However, their hypothesis is based on the different response to different lateral boundary conditions; it does not need the concept of multiple planetary flow regimes.

If we look at the observational result carefully (Tables 2, 3 and 4 in Labitzke, 1982), we notice that there is room for introducing the concept into the interannual variability. That is to say, the observed two regimes are not determined uniquely by the phase of the equatorial QBO, but there are some "exceptional" months even in the same equatorial QBO phase. There exist several undisturbed cold months even in the easterly phase and disturbed warm months even in the westerly phase. The "exceptional" months might be considered as another metastable planetary flow regime under the same lateral boundary condition (i.e., QBO phase). At all events, we have to wait for the accumulation of data and detailed investigations to affirm or to deny our hypothesis of multiple planetary flow regimes in the stratosphere during the northern winter. In the remainder of this section, we discuss some relations to previous theoretical studies on the stratospheric dynamics.

The HM model has the essence of some theories on the stratospheric sudden warmings. The essence of Matsuno's (1971) theory is impulsive initiation of a wave forcing; transient response to the forcing causes deceleration of westerly zonal wind and the sudden warming. This process can be reproduced by a time-integration setting $h_B(t) = h_\infty[1 - \exp(-t/\tau)]$ as in HM, where $\tau = 2.5 \times 10^5$ s. If the asymptotic steady state amplitude of the wave forcing h_∞ is less than a critical value, the time-dependent solution is finally attracted to a stable steady solution A after some migrations due to initial transience (Fig. 8, line 1). On the other hand, if h_∞ is greater than a critical value (Fig. 8, line 2), the initial transience makes it possible to transit from the stable steady solution A to stable periodic solution

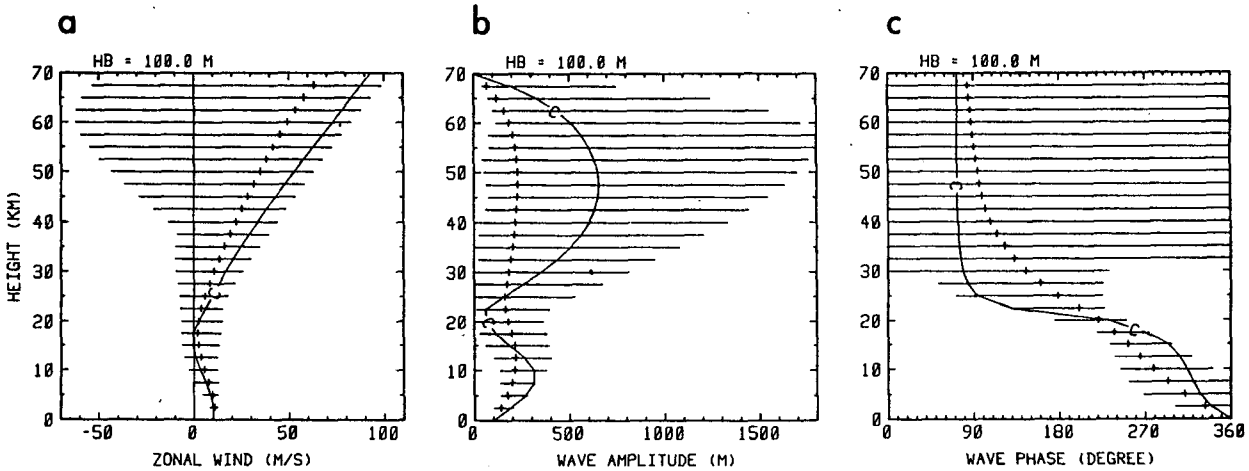

FIG. 6. Vertical profile of the time-averaged state over one vacillation cycle (+) and the range of vacillation (horizontal bar) for h_B = 100 m. Unstable solution C is also shown by a solid line.

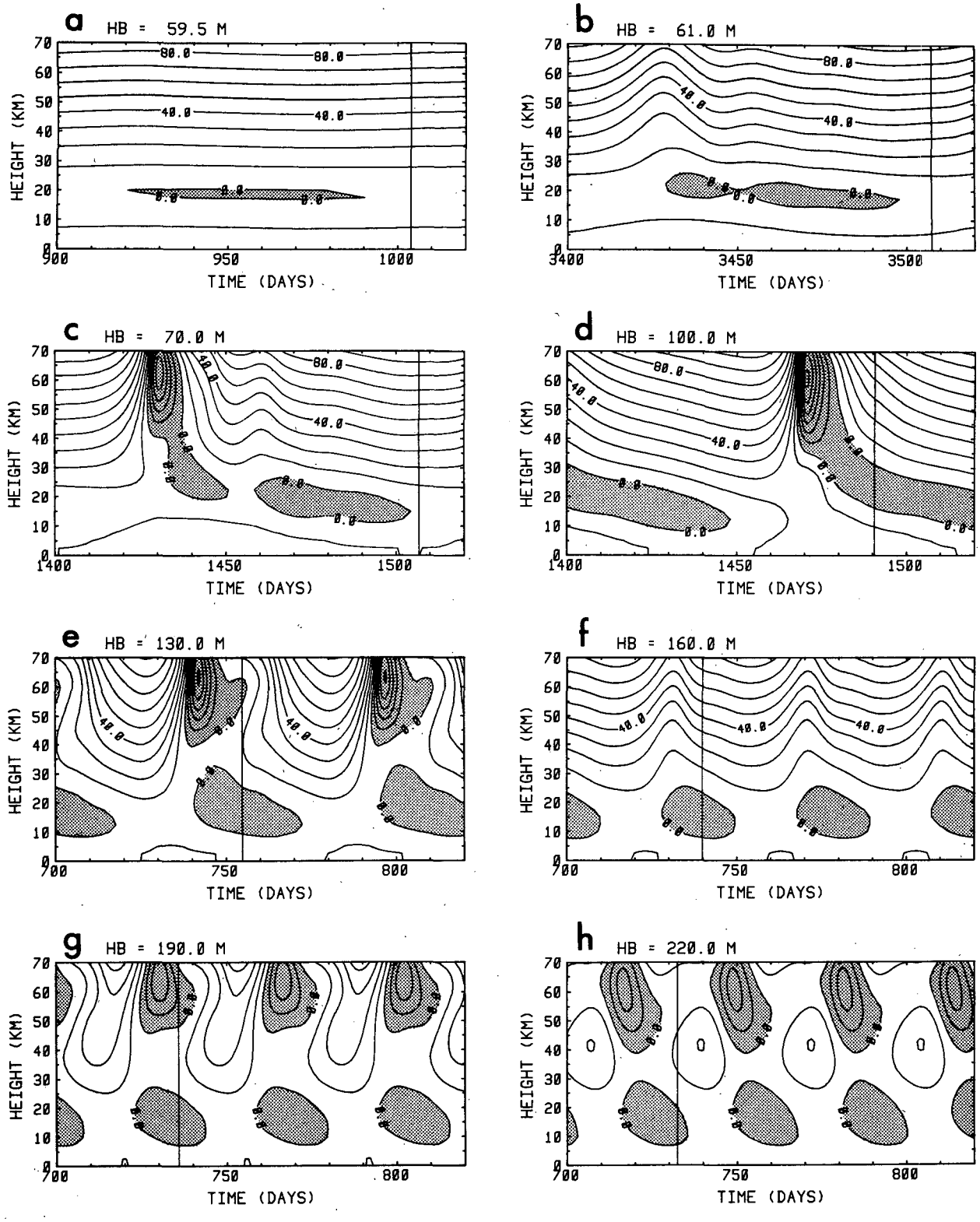

FIG. 7. Time–height sections of the mean zonal wind U [m s^{-1}] of periodic solutions. Westward winds are shaded. Vertical line in each figure denotes one period.

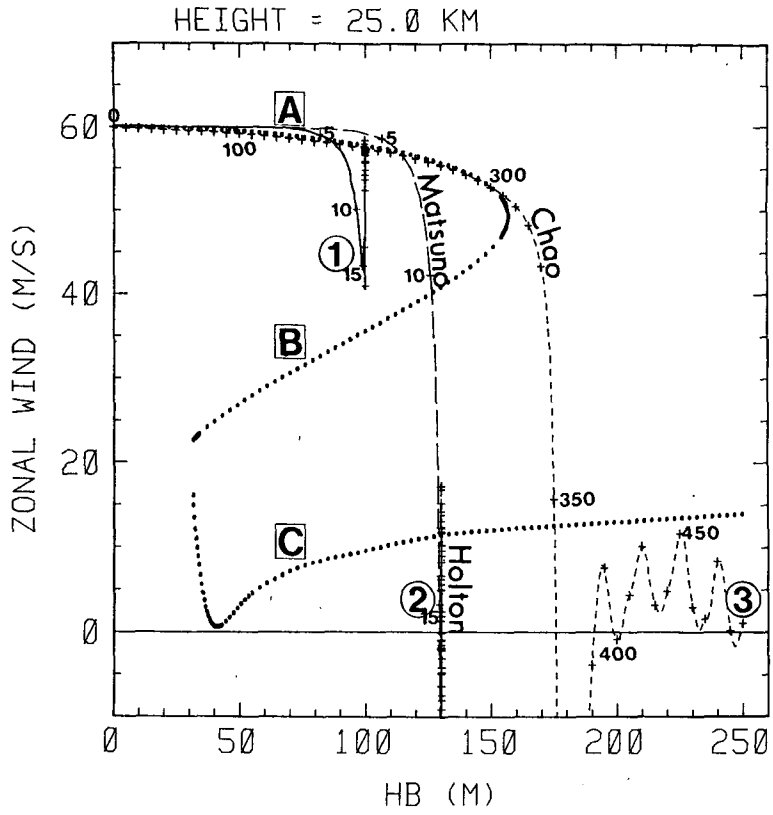

FIG. 8. Trajectories of three time-dependent solutions projected onto $h_B - U(z = 25$ km) plane. Steady solution branches A–C in Fig. 3a are denoted by dotted lines. Three lines (①–③) are responses to different wave forcings. ①: $h_B(t) = 100$ m $\times [1 - \exp(-t/\tau)]$; ②: $h_B(t) = 130$ m $\times [1 - \exp(-t/\tau)]$; ③: $h_B(t) = 0.5$ m day$^{-1} \times t$; where $\tau = 2.5 \times 10^5$ s. Symbol + is put every 5 days for ① and ② and 10 days for ③. Unit of label is written in days.

(vacillation). The transition is interpreted as the sudden warming in the framework of Matsuno's thoery.

Another theory of the sudden warming is the vacillation found by HM. In the case of Fig. 8, line 2, the solution is finally captured by the vacillation labeled "Holton", which is the same as that in Fig. 3 with $h_B = h_\infty = 130$ m. The periodic solutions in Fig. 7c, d, e might be regarded as major warmings. Suddenness is well reproduced in these solutions. The periods of 50–100 days for the vacillations corresponds to the sparseness of warmings (0–2 times a winter). The vacillations exist even in the presence of steady forcing.

The catastrophe theory by Chao (1985) is also illustrated in Fig. 8, (line 3). Because linear increase of a wave forcing in time is set to a small value (0.5 m day^{-1}), the time-dependent solution follows up the stable steady solution branch A. However, when it exceeds the limit point L (Fig. 3), there takes place a transition to vacillation branch. Large magnitude of transient forcing as in Matsuno's theory is not necessary for the transition due to catastrophe. Quasi-static increment of the forcing is enough for this process.

The fundamental dynamics of the multiple flow equilibria in Charney and DeVore's model is nonlinear resonance. Although the lower boundary condition in the HM model (2.9) is not originally suitable for discussing resonance, it is interesting to investigate the wave response to different zonal flow forcings. Because the linear resonance theory in the presence of vertical shears shows that there may be an infinite number of resonant wind configurations (Tung and Lindzen, 1979), one parameter of the zonal wind forcing (U_{RB} or Λ in (2.7) for this study) is enough to know the wave response in relation to the resonance.

Figure 9 shows the bifurcation diagram for the parameter U_{RB}. The solution branches in the wave amplitude bring hope of relating the result in the present study to the resonance theory; the wave response has a large amplitude around $U_{RB} = 13$ m s^{-1}. However, vertical profiles of five steady solutions for $U_{RB} = 13$ m s^{-1} (Fig. 10) do not show any feature that reminds us of the resonance. For example, the wave phase of the "subresonant" solution (B) is not much different from that of the "super-resonant" solutions (D, E)

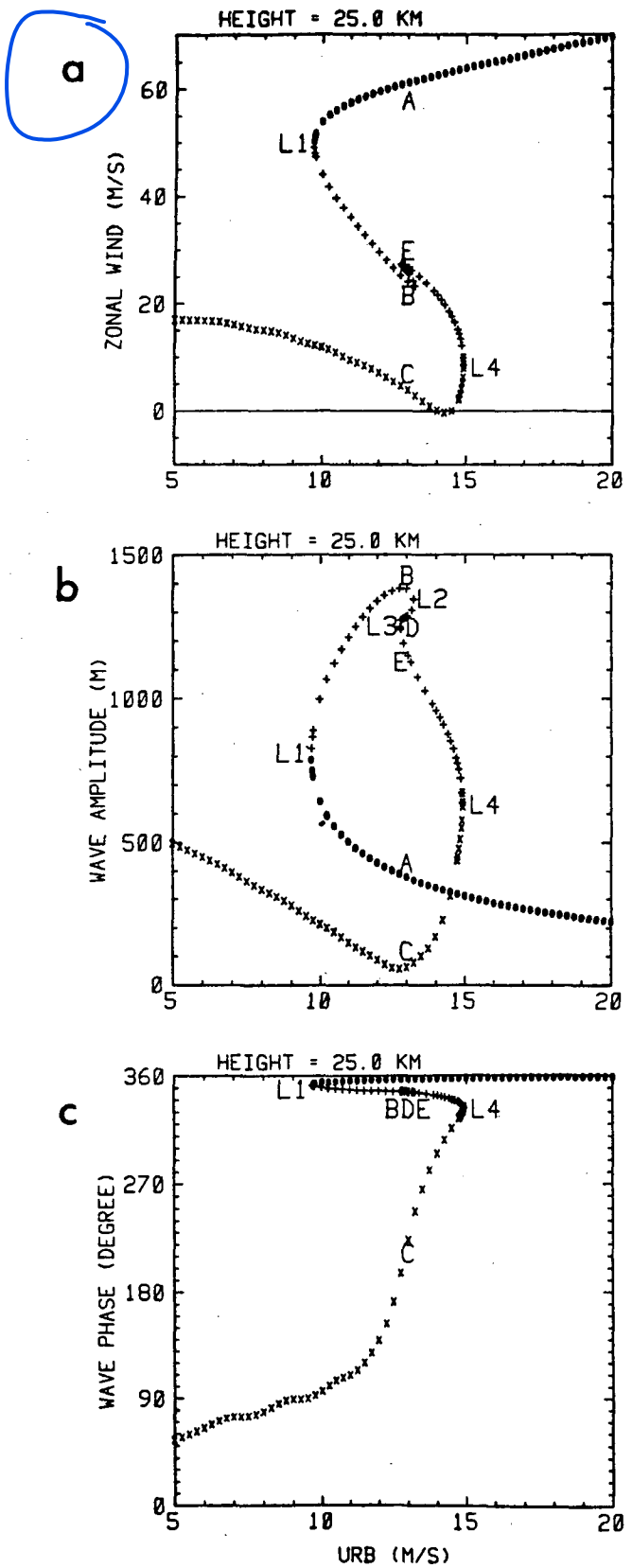

contrary to the out-of-phase relation in the resonance theory. It is concluded that the nonlinear resonance is not a good interpretation for the multiple stable solutions in the HM model. The difference in the lower boundary condition is crucial for the different wave response.

There are several kinds of interference theory (Lindzen et al., 1982; Robinson, 1985; Salby and Garcia, 1987) and instability theory (Plumb, 1981) for the explanation of vacillations (mainly in the stratosphere). Some aspects of the vacillations in the HM model show apparent resemblance to some of theirs. However, detailed experiments and considerations are necessary to apply these theories to the vacillations in the HM model, because the first assumptions, for example, the lower boundary conditions, are different between these studies.

6. Conclusion

Bifurcation properties of the stratospheric vacillation model introduced by Holton and Mass (1976) were investigated in view of application to the climatology of planetary scale flow in the stratosphere. The Holton and Mass model, which describes the wave–zonal flow interaction under a constant wave forcing at the bottom boundary, was decomposed into a set of 81 nonlinear ordinary differential equations with variables depending on time.

If we take the wave forcing as a bifurcation parameter, we obtain three branches of the steady solutions. Linear stability analysis of these steady solutions shows that two stable solutions coexist in some range of the wave forcing: one of the stable solutions is close to the radiative equilibrium; the other has a larger wave amplitude and a weaker mean zonal wind in the lower layers.

The periodic solutions branch off a steady solution by a Hopf bifurcation. These solutions are comprised of several kinds of stratospheric vacillations; i.e., a series of minor, or major, stratospheric warmings. There exists a multiplicity of stable solutions (steady solutions close to the radiative equilibrium and vacillating solutions) in some other range of the wave forcing.

Except for the vicinity of the Hopf bifurcation point, the time average of the periodic solutions over one vacillation cycle is significantly different from the unstable steady solution (the original branch of the periodic solutions). The difference comes from the nonlinear transience term.

FIG. 9. As in Fig. 3 but for another bifurcation parameter U_{RB} under fixed values of h_B = 145 m and Λ = 2 m s^{-1}/km. Limit points are denoted by L1–L4. Vertical profile of the steady solutions A–E at U_{RB} = 13.0 m s^{-1} are shown in Fig. 9.

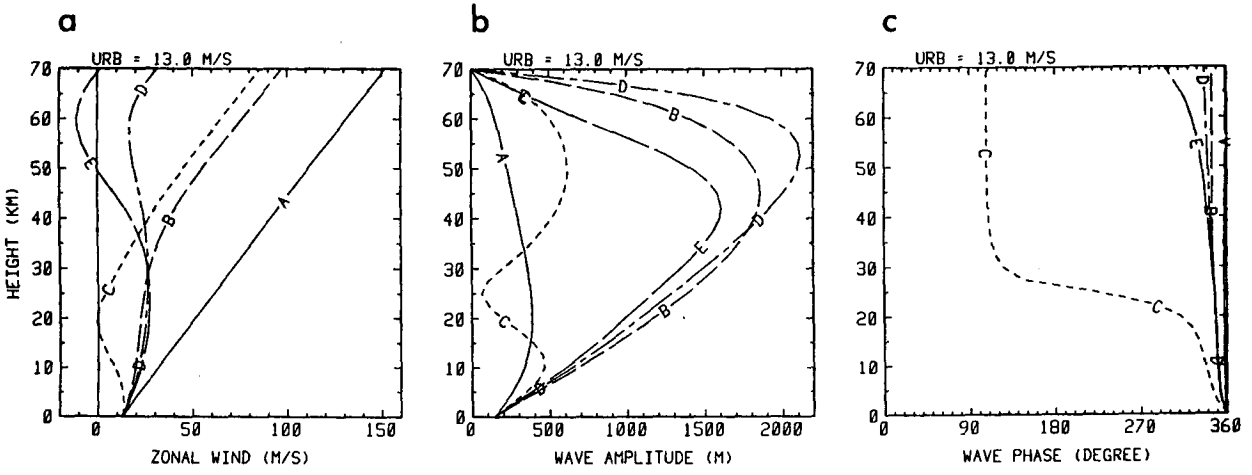

FIG. 10. As in Fig. 2 but for h_B = 145 m, Λ = 2 m s^{-1} km^{-1} and U_{RB} = 13.0 m s^{-1}.

Acknowledgments. The author wishes to thank J. R. Holton for his helpful discussions. This work was supported in part by the National Aeronautics and Space Administration, NASA Grant NAGW-662.

REFERENCES

Boville, B. A., 1986: Wave-mean flow interactions in a general circulation model of the troposphere and stratosphere. *J. Atmos. Sci.*, **43,** 1711–1725.

Chao, W. C., 1985: Sudden stratospheric warmings as catastrophes. *J. Atmos. Sci.*, **42,** 1631–1646.

Charney, J. G., and J. G. DeVore, 1979: Multiple flow equilibria in the atmosphere and blocking. *J. Atmos. Sci.*, **36,** 1205–1216.

Holton, J. R., and C. Mass, 1976: Stratospheric vacillation cycles. *J. Atmos. Sci.*, **33,** 2218–2225.

——, and T. J. Dunkerton, 1978: On the role of wave transience and dissipation in stratospheric mean flow vacillations. *J. Atmos. Sci.*, **35,** 740–744.

——, and H. C. Tan, 1980: The influence of the equatorial quasi-biennial oscillation on the global circulation at 50 mb. *J. Atmos. Sci.*, **37,** 2200–2208.

——, and ——, 1982: The quasi-biennial oscillation in the Northern Hemisphere lower stratosphere. *J. Meteor. Soc. Japan,* **60,** 140–148.

Labitzke, K., 1977: Interannual variability of the winter stratosphere in the Northern Hemisphere. *Mon. Wea. Rev.*, **105,** 762–770.

——, 1982: On the interannual variability of the middle stratosphere during the northern winters. *J. Meteor. Soc. Japan,* **60,** 124–139.

Legras, B., and M. Ghil, 1985: Persistent anomalies, blocking and variations in atmospheric predictability. *J. Atmos. Sci.*, **42,** 433–471.

Lindzen, R. S., B. Farrell and D. Jacqmin, 1982: Vacillations due to wave interference: Applications to the atmosphere and to annulus experiments. *J. Atmos. Sci.*, **39,** 13–23.

Lorenz, E. N., 1968: Climatic determinism. *The Causes of Climatic Change, Meteor. Monogr.*, No. 30, Amer. Meteor. Soc., 1–3.

Matsuda, Y., 1983: Classification of critical points and symmetry-breaking in fluid phenomena and its application to dynamic meteorology. *J. Meteor. Soc. Japan,* **61,** 771–788.

Matsuno, T., 1971: A dynamical model of the stratospheric sudden warming. *J. Atmos. Sci.*, **28,** 1479–1494.

Plumb, R. A., 1981: Instability of the distorted polar night vortex: A theory of stratospheric warmings. *J. Atmos. Sci.*, **38,** 2514–2531.

Robinson, W., 1985: A model of the wave 1–wave 2 vacillation in the winter stratosphere. *J. Atmos. Sci.*, **42,** 2289–2304.

Salby, M. L., and R. R. Garcia, 1987: Vacillations induced by interference of stationary and traveling planetary waves. Submitted to *J. Atmos. Sci.*

Tung, K. K., and R. S. Lindzen, 1979: A theory of stationary long waves. Part II: Resonant Rossby waves in the presence of realistic vertical shears. *Mon. Wea. Rev.*, **107,** 735–750.

Yoden, S., 1985: Multiple stable states of quasi-geostrophic barotropic flow over sinusoidal topography. *J. Meteor. Soc. Japan,* **63,** 1031–1045.